Nanoscale Advances

ROYAL SOCIETY OF CHEMISTRY

PAPER

View Article Online
View Journal | View Issue

Cite this: *Nanoscale Adv.*, 2021, **3**, 5676

Anomalously polarised emission from a MoS_2/WS_2 heterostructure†

P. Riya Mol, Prahalad Kanti Barman, Prasad V. Sarma, Abhishek S. Kumar, Satyam Sahu, Manikoth M. Shaijumon and Rajeev N. Kini *

Received 21st June 2021
Accepted 17th August 2021

DOI: 10.1039/d1na00462j

rsc.li/nanoscale-advances

We report circularly polarised emission, with helicity opposite to the optical excitation, from a van der Waals heterostructure (HS) consisting of a monolayer MoS_2 and three-layer WS_2. Selective excitation of the MoS_2 layer confirms that this cross-polarized emission is due to the charge transfer from the WS_2 layers to the MoS_2 layer. We propose that the high levels of n-doping in the constituent layers due to sulphur vacancies and defects give rise to an enhanced transition rate of electrons from the *k* valley of WS_2 to the *k*′ valley of MoS_2, which leads to the emission, counter polarized to the excitation. Simulations based on the rate equation model support this conclusion.

1. Introduction

Two-dimensional van der Waals heterostructures (HSs) made up of atomically thin layers of transition metal dichalcogenides (TMDs) have emerged as a platform for exploring spin and valley physics and its applications.[1,2] Many of these HSs have a type II band alignment, leading to efficient and ultrafast separation of the photoexcited electrons and holes into the different layers.[3–5] This makes the HSs particularly interesting for light-harvesting applications. In HSs, the electrons and holes are separated in both the real and the momentum space, giving rise to a long valley lifetime.[6–8] Hence, TMD HSs are promising also for valleytronics applications. The separation of the charges in different layers gives rise to interlayer excitons (IXs).[9–12] There have been extensive studies focussing on the IXs[9–12] as well as intralayer excitons.[3,13]

The HSs inherit the interesting spin–valley physics of the constituent layers and lead to numerous intriguing phenomena. Due to the large spin–orbit coupling and entangled spin and valley degrees of freedom (DoF), TMDs provide a unique platform to manipulate valley pseudospin through circularly polarized light.[14,15] Due to the valley contrasting Berry curvature and magnetic moment, the valley DoF can be manipulated using a magnetic field.[16–19] Additionally, the valley splitting can be enhanced by more than an order of magnitude by taking advantage of antiferromagnetic substrates' magnetic proximity coupling.[20] Doping provides another exotic way to control the exchange interactions in TMDs, leading to giant and tunable valley splitting in TMDs. TMDs grown by the chemical vapour deposition (CVD) method have a high density of chalcogen vacancies. In HSs with type-II band alignment, the electrons and holes get localized in different layers *via* ultrafast charge transfer.[3] It has been shown that this leads to a dramatic enhancement in the exchange interaction along with an anomalous enhancement in the *g*-factor.[13] The ultrafast charge transfer in TMD HSs also provides an all-optical route to control spin–valley phenomena by tuning the doping concentration by varying the laser power.[13]

Another interesting feature of TMDs, due to the valley-degenerate spin-contrasting bandstructure, is that they host both optically active and inactive intravalley excitons, called bright and dark excitons, respectively.[21–24] In Mo-based monolayer TMDs, the ground state is a bright exciton, and the dark state lies energetically above it. Though most of the studies on TMDs focused on bright excitons, the existence of dark excitons has been experimentally probed *via* different techniques.[25–27] Dark excitons are highly interesting, and many of the optical properties strongly depend on the competition between the bright and dark exciton states. Experiments have shown that the application of a magnetic field can brighten the dark exciton states.[26–30] Plasmon induced brightening of dark excitons in the TMDC monolayer has also been reported.[31] In doped TMD layers, trions (charged excitons) are also formed along with excitons. The application of a magnetic field has been shown to brighten the corresponding dark (charged) excitons.[28] Intriguingly, the emission from the brightened dark exciton states showed helicity opposite to that of the excitation.[28] However, in TMD HSs, even though IXs with helicity opposite to the excitation have been reported, reversing the helicity of intralayer exciton emission has not been reported, and intralayer excitons preserve the helicity of the excitation light. We report circularly polarised intralayer exciton emission, with helicity opposite to the optical excitation, from a MoS_2/WS_2 heterostructure.

Indian Institute of Science Education and Research Thiruvananthapuram (IISER TVM), Maruthamala P. O. Vithura, Kerala 695551, India. E-mail: rajeevkini@iisertvm.ac.in

† Electronic supplementary information (ESI) available. See DOI: 10.1039/d1na00462j

Selective excitation of the MoS_2 layer confirms that this cross-polarized emission is due to the charge transfer from the WS_2 layers to the MoS_2 layer. We propose that a dark exciton state in the MoS_2 layer gets brightened due to n-doping, and the anomalous polarization arises due to the charge transfer from the conduction band of WS_2 to this brightened dark exciton state. We provide simulations based on the rate equation model to support this conclusion.

2. Sample growth and characterisation

The WS_2/MoS_2 HS was synthesised on a Si/SiO_2 substrate *via* single-step chemical vapour deposition (CVD) at 900 °C using a Thermo Scientific Lindberg Blue M split-tube furnace. First, WO_3 powder (Aldrich puriss 99.9%) is dispersed in ethanol (0.2 mg mL^{-1}), and 10 μL dispersion is drop coated to each cleaned substrate. Similarly, MoO_3 powder is dispersed in ethanol at a similar concentration. After drying the WO_3 dispersion, 10 μL of MoO_3 dispersion is drop coated on the same substrate. Once dried in air, these substrates were loaded at the centre of the tubular furnace. As the sulfur source, 500 mg sulfur powder (Aldrich, purum 99.5%) is placed at the upstream end of the tube, just outside the heating elements. The tube is flushed several times using ultra-high-pure argon gas before the deposition to remove moisture/oxygen from the furnace. The heterostructure growth was observed at a temperature of 900 °C after a dwell time of 10 minutes while maintaining 200 sccm argon flow throughout the experiment.

Temperature-dependent and helicity resolved photoluminescence (PL) was performed using a homebuilt micro-PL setup in the backscattering configuration. For PL measurements, a 532 nm solid-state laser with an average laser power of 3.5 mW was used as the excitation source. The excitation light was focused on the sample using a 10× objective lens (NA = 0.24) which gave a spot size of ≈3 μm-diameter. The signals were collected with the same objective lens, analysed using a 0.32 m monochromator (Horiba-Jobin Yvon iHR320) and detected with a thermoelectrically cooled CCD camera. The experiments were performed at different temperatures in the range of 16–300 K using an ultralow vibration closed-cycle refrigerator. The PL and Raman maps were obtained using a Raman microscope (XploRa PLUS, Horiba Scientific) with 532 nm laser excitation. A 50× microscope objective (NA = 0.8) was used, and it gave a spot size of ≈1 μm-diameter on the sample during PL mapping.

An atomic force microscope (AFM) image of the HS is shown in Fig. 1(a). The sample has a three-layer (3L) thick hexagonal base (WS_2) with a triangular monolayer (ML) on top of it (MoS_2), as indicated by the dotted lines in Fig. 1(a). The thickness of the WS_2 and MoS_2 layers is confirmed using AFM line scans, as shown in the inset of Fig. 1(a). It has been reported earlier that in WS_2, compared to ML, even though the emission is weaker in thicker flakes, thicker flakes give rise to a higher degree of polarization.[32,33] Hence we have chosen a 3L thick WS_2 to form the HS. The top panel of Fig. 1(b) shows the PL from the triangular heterostructure region, which is similar to what has been reported earlier.[3,12,13,34] The PL spectra obtained from a CVD grown ML-MoS_2 and a 3L-WS_2 is also shown in Fig. 1(b) for reference. The PL spectra from HS show two peaks, an intense peak close to the charged exciton peak (AX^-) in MoS_2 (X_M) and a second peak at higher energy (X_W). The dominant peak X_M near the MoS_2 AX^- peak indicates that the HS is highly doped, and the peak position agrees with the previous reports on unintentionally doped MoS_2/WS_2 HS.[13,35] The X_W peak is close to the emission peak observed in 3L-WS_2 and the B-exciton (BX) in ML-MoS_2. It has been reported that the PL from the HS is an additive spectrum of emission from the constituent WS_2 and MoS_2 layers in the ratio 1 : 5–10.[5,34] We believe that the X_W consists of contributions from both the exciton emission of WS_2 and the BX emission of MoS_2. In this paper, we focus on the X_M emission peak. Fig. 1(c) and (d) show the 2D map of the emission intensity near X_M and X_W. It can be seen that the emission from the triangular heterostructure region has a peak near X_M, and the X_W emission is observed from the whole sample, including the 3L-WS_2 base. The Raman and PL intensity maps confirm that the MoS_2 layer is present only in the triangular region, as indicated in Fig. 1(a).

Fig. 1(e) shows the Raman signals from the top of the heterostructure and the edge of the sample. The Raman signal from the top of the heterostructure consists of peaks corresponding to the in-plane (E^1_{2g}) and out-of-plane (A_{1g}) modes of MoS_2 and WS_2. The Raman signal from the edge of the sample shows only (E^1_{2g}) and (A_{1g}) modes corresponding to the WS_2 layer, confirming that the hexagonal base consists of WS_2, and MoS_2 is present only in the triangular region. Apart from the E^1_{2g} and A_{1g} modes, there are two other modes, marked U1 and U2 in ESI Fig. S1,† which appear both in the heterostructure region and the edge of the sample. However, their origin is not clear at this point. Fig. 1(f) shows the 2D map of the A_{1g} mode of WS_2. In the triangular HS region, A_{1g} of WS_2 shows a slight decrease in intensity due to the presence of the MoS_2 layer. Hence, we confirm that the heterostructure consists of a hexagonal 3L-WS_2 with a triangular ML-MoS_2 on top of it.

3. Results and discussion

We studied the polarisation characteristics of the emission from the HS. The HS was excited with a circularly polarised laser at 532 nm, and the polarisation of the PL emission was analysed. Fig. 2(a) shows the PL emission from the heterostructure at room temperature and low temperature (≈16 K) upon excitation with right-circularly polarised light (σ^+). At room temperature, the X_W peak is predominantly co-polarised (σ^+) with the excitation, while the X_M is cross-polarised (σ^-) with the excitation. The peaks are blue-shifted at low temperature; however, similar polarisation dependence is observed; the X_M peak is cross-polarised (σ^-), and the X_W peak is co-polarised (σ^+) with the excitation. Again same polarization characteristics were observed upon excitation with left-circularly polarised light (σ^-), as shown in ESI Fig. S1.†

We define the degree of circular polarisation (DCP) as $\rho = (I_+ - I_-)/(I_+ + I_-)$, where I_+ (I_-) denotes the intensity of the PL

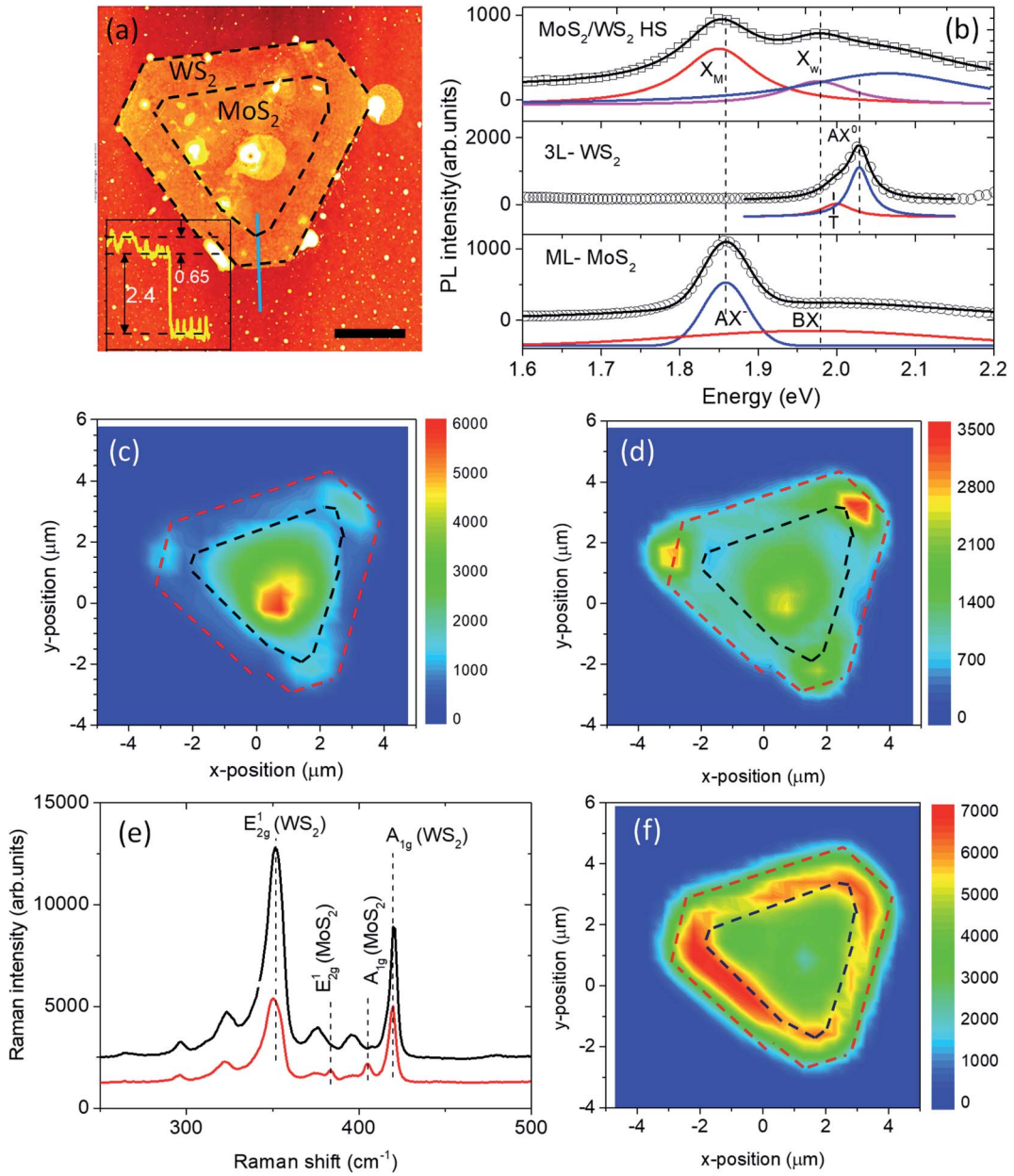

Fig. 1 (a) Atomic force microscope image of the MoS_2/WS_2 heterostructure (HS). The dashed lines indicate the boundary of the constituent WS_2 and MoS_2 layers. The scale bar is 2 microns. Inset shows the line profile along an edge of the sample indicated by the grey line (b) low temperature ($T = 17$ K) PL spectra from MoS_2/WS_2 HS (top panel), 3L-WS_2 (middle panel) and ML-MoS_2 (bottom panel) obtained using 532 nm, linearly polarized excitation. The open symbols are the experimental data; the solid black lines are obtained by fitting the peaks to Lorentzian. The red, blue and pink lines represent the individual Lorentzian peaks. The data and the Lorentzian peaks are offset vertically for clarity. PL intensity map of (c) X_M and (d) X_W peaks in the HS sample. (e) Raman signal from the top (red) and edge (black) of the HS sample. (f) Raman intensity map of the A_{1g} peak of the HS sample.

component co-polarized (cross-polarized) with the excitation. DCP is plotted in the bottom panel of Fig. 2(a), and it can be seen that the DCP is negative near X_M. Similar measurements were performed on individual ML MoS_2 and 3L WS_2 flakes, shown in supplementary Fig. S2.† The ML MoS_2 and the 3L WS_2 flakes do not show this anomalous counter polarisation for the emission, which agree with earlier reports.[14,32,36–38] Fig. 2(b) shows the temperature dependence of the DCP near X_M and X_W peaks. For reference, the temperature dependence of the DCP of AX^- emission from ML-MoS_2 is also shown in Fig. 2(b). It can be seen that the DCP near the X_W peak in the HS at all temperatures, even though very low ($\approx$1–4%), remains positive, and the DCP remains negative for the X_M peak. DCP measurements have been reported earlier on MoS_2/WS_2 HSs, and interlayer excitons have been shown to have negative DCP.[10,11,13] However, intralayer exciton emission has not been reported to show negative DCP.[10,13] Most of the earlier work was reported on HSs comprising of MLs of MoS_2 and WS_2.[3,12,13,34] Hence, we first look

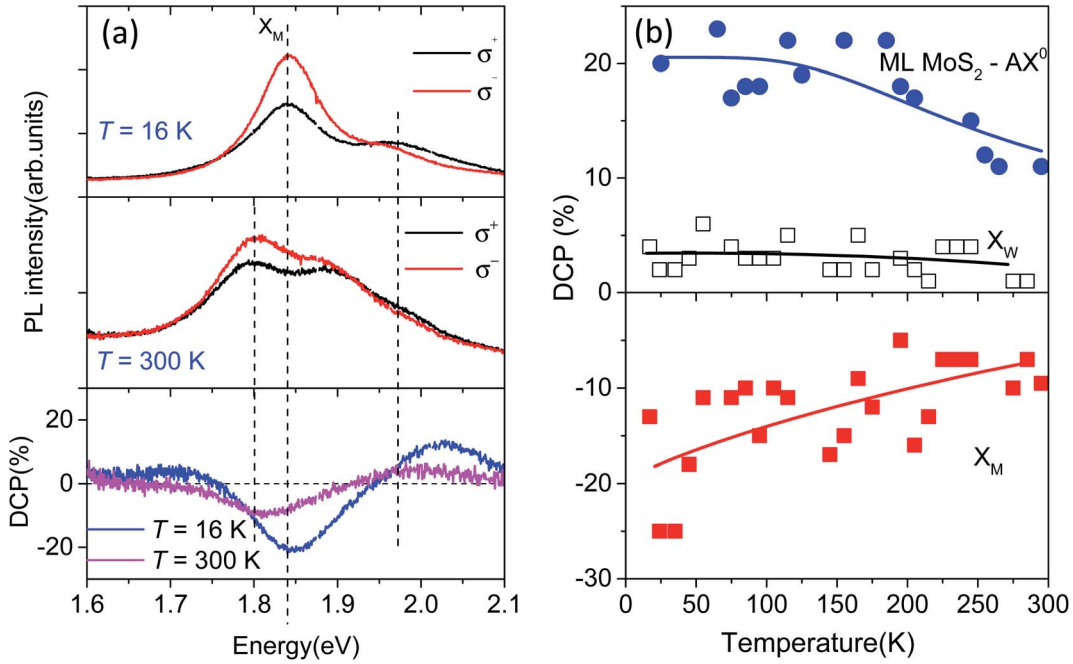

Fig. 2 (a) Helicity resolved PL spectra obtained from the MoS_2/WS_2 HS with 532 nm, circularly polarized (σ^+) excitation at $T = 16$ K (top panel) and $T = 300$ K (middle panel). Degree of polarization (DCP) at $T = 16$ K and $T = 300$ K (bottom panel) obtained with 532 nm, σ^+ excitation of the MoS_2/WS_2 HS. (b) DCP near the X_M and X_W peaks, at different temperatures, obtained with 532 nm, σ^+ excitation of the MoS_2/WS_2 HS. The DCP data corresponding to the charged exciton (AX^-) in ML-MoS_2 are also shown in the top panel. The solid lines are a guide for the eye.

at the possibility of the negative DCP to be due to the different layer structure used here, *i.e.*, 3L-WS_2 and ML-MoS_2.

Even though density functional theory (DFT) often underestimates the bandgap, it can provide necessary information for distinguishing different excitations in different heterostructures. We computed the bandstructure of the HS consisting of 3L-WS_2 and ML-MoS_2 using DFT (see ESI Note 1† for details) and compared it with the bandstructure of the well-studied HS comprising MLs of MoS_2 and WS_2 in ESI Fig. S3.† The band structure calculations demonstrate type-II band alignment.[4,5] Compared to the HS with ML-WS_2, for the HS with 3L-WS_2, the band minimum at the *Q*-point is further lowered, and the VB maximum at the *Γ*-point is further pushed up.[12,13,34] Hence the IX is at much lower energy than what has been observed in the literature and is beyond the spectral range accessible in our measurements. However, the band minima near *K*-points are very similar in both the HSs. Hence, the difference in the polarization behaviour of X_M emission cannot be attributed to the changes in the band structure.

We first conducted measurements with a 633 nm (1.96 eV) laser excitation to understand the origin of this cross-polarised emission. 633 nm laser allowed us to selectively excite the MoS_2 layer in the HS and ensure that the WS_2 layers were not populated. The helicity resolved PL and DCP from the HS at 17 K with 633 nm, σ^+ polarized excitation is shown in Fig. 3. It can be seen that with 633 nm excitation, the DCP of the X^M peak is positive. Similar behaviour was obtained with σ^- polarized 633 nm excitation as shown in ESI Fig. S4(a).† Positive DCP was obtained for all temperatures up to room temperature, with 633 nm excitation as shown in ESI Fig. S4(b).† The absence of negative DCP when WS_2 is not populated confirms that the negative DCP arises from the transfer of electrons from the WS_2 layer to the MoS_2 layer.

After the excitation of the HS layers, charge transfer occurs, mostly *via* spin-conserving transfers to the lowest energy band, irrespective of the interlayer momentum mismatch.[10] So the excitation of the WS_2 layer with σ^+ polarized light and subsequent charge transfer could lead to the population of the spin-up state in the *k* valley of MoS_2, which would result in the emission of σ^+ polarized light. However, negative DCP results

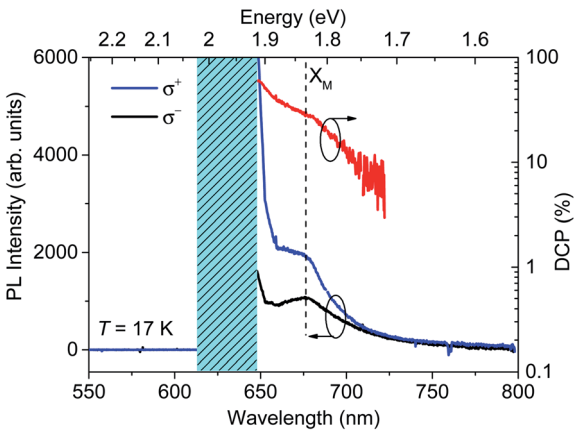

Fig. 3 Helicity resolved PL spectra and degree of polarization (DCP) obtained from the MoS_2/WS_2 HS with 633 nm, circularly polarized (σ^+) excitation at $T = 17$ K. The shaded blue region indicates the stopband of the filter used to block the laser light from reaching the detector.

from the dominant emission of σ^- polarized light. Negative DCP indicates that interlayer scattering results in the enhanced exciton population in the k' valley of MoS_2, which would give rise to the emission of σ^- polarized light. To examine this possibility, we use a rate equation model as described below. A schematic of the band structure and the spin configuration is shown in Fig. 4(a). The system of rate equations for the WS_2/MoS_2 HS can be written as follows:

$$\frac{dN_w}{dt} = g - \frac{N_w}{\tau_r^w} - \frac{N_w}{\tau} - \frac{N_w}{\tau'}$$

$$\frac{dN_{Mo}}{dt} = g - \frac{N_{Mo}}{\tau_r^{Mo}} + \frac{N_w}{\tau} - \frac{N_{Mo}}{\tau_s^{Mo}} - \frac{N'_{Mo}}{\tau_s^{Mo}}$$

$$\frac{dN'_{Mo}}{dt} = g' - \frac{N'_{Mo}}{\tau_r^{Mo}} + \frac{N_w}{\tau'} + \frac{N_{Mo}}{\tau_s^{Mo}} - \frac{N'_{Mo}}{\tau_s^{Mo}}$$

N_{Mo} (N'_{Mo}) is the exciton population in the k (k') valley of the MoS_2 layer and N_w the exciton population in the k valley of the WS_2 layer. g (g') is the generation rate in the k (k') valley, which is assumed to be a constant for continuous-wave excitation. We assumed that σ^+ excitation generates excitons in the k valleys of MoS_2 and WS_2 layers, and for simplicity, we have ignored the scattering of electrons to the k' valley of the WS_2 layer. This assumption is valid since, due to the type-II band alignment, the transfer of photogenerated electrons from the WS_2 k valley to the MoS_2 valleys is more efficient than their scattering to the k' valley of the WS_2.[39] τ_s^{Mo} and τ_r^{Mo} represent the intervalley scattering time and the radiative recombination time, respectively, in the MoS_2 layer. τ_r^w represents the radiative recombination time in the WS_2 layer. τ (τ') represents the intralayer scattering time between the k valley in WS_2 and the k (k') valley in MoS_2. The polarization state is calculated under steady-state conditions $\left(\frac{dN_w}{dt} = \frac{dN_{Mo}}{dt} = \frac{dN'_{Mo}}{dt} = 0\right)$. The DCP of the X_M emission is related to the population of exciton states in the k (k') valleys of MoS_2,

$$\rho = \frac{N_{Mo} - N'_{Mo}}{N_{Mo} + N'_{Mo}}$$

Solving the above set of rate equations for $g = 1$ and $g' = 0$ we obtain

$$\rho = \frac{\gamma_r^{Mo}(\gamma(1-\alpha)+1)}{(2+\gamma_r^{Mo})(\gamma(1+\alpha)+1)}$$

where $\gamma_r^{Mo} = \frac{\tau_s^{Mo}}{\tau_r^{Mo}}$ and $\gamma = \frac{\tau_s^{Mo}}{\tau}$ represent the relaxation rates and $\alpha = \frac{\tau}{\tau'}$.

If we ignore the interlayer scattering ($\gamma = 0$), the above equation describes an isolated MoS_2 layer, and it reduces to $\rho = \frac{1}{1+\frac{2}{\gamma_r^{Mo}}} = \frac{1}{1+2\frac{\tau_r^{Mo}}{\tau_s^{Mo}}}$.[40] In that case, we obtain $\rho \approx 20\%$ for $\gamma_r^{Mo} \approx 1/2$, which agrees with the ρ obtained for ML-MoS_2 at low temperature. $\tau_r^{Mo/W}$ is in the range of picoseconds to hundreds of picoseconds.[25,41,42] The intervalley scattering time τ_s^{Mo} depends on the excitation energy but will be of the same order of $\tau_r^{Mo/W}$.[40] It has been shown that the interlayer scattering time (τ', τ) is of the order of 50–450 fs (ref. 3, 34, 43 and 44) which means γ, $\gamma' > 1$. Fig. 4(b) shows ρ as a function of α for $\gamma_r^{Mo} = 1/2$ and for different values of γ, which shows that negative DCP is indeed possible for $\tau' < \tau$. This means that electrons photoexcited to the k valley of WS_2 by σ^+ polarised light are scattered preferentially to the k' valley compared to the k valley of MoS_2. We believe that this is due to unintentional doping of the HS. CVD grown samples have a high density of sulphur vacancies, leading to high levels of n-doping which is evident from the emission X_M near the charged exciton energy in MoS_2.[13] The high levels of n-doping has two effects. Firstly, the Fermi level will be located in the spin-split upper conduction band of MoS_2.[13] Because of this, the electrons from WS_2 layers will be scattered to the spin-split upper conduction bands of MoS_2. The transition to the spin-split upper conduction band of MoS_2 k' valley ($m_j = -3/2$) would be a spin-conserving transition. Hence, possibly, the transition rate of this spin-conserving transition is enhanced compared to the spin-flip

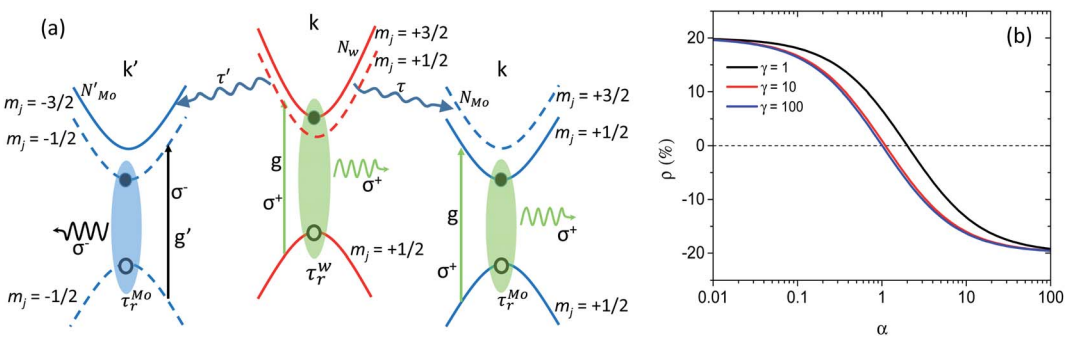

Fig. 4 (a) A schematic of the different bands in the MoS_2/WS_2 HS. Solid and dotted lines represent bands with different spin configurations. The bands are labelled with the z-component of their total angular momentum, m_j. Vertical arrows indicate optical excitations: black and green arrows correspond to σ^- and σ^+ excitation, respectively. The black and green wiggly arrows indicate σ^- and σ^+ emission, respectively. The gray wiggly arrows represent spin-conserving interlayer transfer to the lowest energy band. (b) Degree of circular polarization, ρ, calculated using the rate equation model described in the main text for $\gamma_r^{Mo} = 1/2$ and different values of α.

transition to the k valley (m_j = +3/2). Normally, the spin-conserving transition from WS_2 to the spin-split upper conduction band of the MoS_2 k' valley would give rise to dark (neutral or charged) excitons. However, as another consequence of the n-doping of the layers the dark exciton state is brightened, similar to the brightening observed earlier for the dark IX state in MoS_2/WS_2 HSs due to electrostatic doping.[9]

4. Conclusions

In conclusion, we unveil anomalous polarization from a van der Waals heterostructure (HS) consisting of ML-MoS_2 and 3L-WS_2. Selective excitation of the MoS_2 layer in the HS demonstrates that this anomalous polarization originates from the charge transfer from WS_2 to MoS_2 layers. We propose that due to high levels of n-doping in the layers, caused by sulphur vacancies and defects, the transition rate of electrons from the k valley of WS_2 to the k' valley of MoS_2 is enhanced, which leads to emission, counter polarized (σ^-) to the excitation (σ^+). We simulated this scenario using a set of coupled rate equations, and the simulations agree well with our experimental observations. Our measurements provide new prospects to control the helicity of the emission from van der Waals HSs *via* doping.

Author contributions

PRM and PKB did the measurements and analysed the data. PVS grew the samples. ASK did the DFT calculations. SS did the simulations based on the rate equation model. MMS designed and supervised the growth of nanostructures. RNK supervised the measurements & analysis and prepared the manuscript with inputs from all co-authors.

Conflicts of interest

The authors declare that they have no known competing financial interests or personal relationships that could have appeared to influence the work reported in this paper.

Acknowledgements

RNK acknowledges the funding support by the Science and Engineering Research Board, Department of Science and Technology, India, through the Research Grant No. CRG/2019/004865 and IPA/2020/000021. The support for computing time at the IISER Thiruvananthapuram HPC cluster "Padmanabha" is also kindly acknowledged.

References

1 A. K. Geim and I. V. Grigorieva, Van der Waals heterostructures, *Nature*, 2013, **499**, 419–425.
2 P. Rivera, H. Yu, K. L. Seyler, N. P. Wilson, W. Yao and X. Xu, Interlayer valley excitons in heterobilayers of transition metal dichalcogenides, *Nat. Nanotechnol.*, 2018, **13**, 1004–1015.
3 X. Hong, J. Kim, S. F. Shi, Y. Zhang, C. Jin, Y. Sun, S. Tongay, J. Wu, Y. Zhang and F. Wang, Ultrafast charge transfer in atomically thin MoS_2/WS_2 heterostructures, *Nat. Nanotechnol.*, 2014, **9**, 682–686.
4 J. Kang, S. Tongay, J. Zhou, J. Li and J. Wu, Band offsets and heterostructures of two-dimensional semiconductors, *Appl. Phys. Lett.*, 2013, **102**, 12111.
5 H. P. Komsa and A. V. Krasheninnikov, Electronic structures and optical properties of realistic transition metal dichalcogenide heterostructures from first principles, *Phys. Rev. B: Condens. Matter Mater. Phys.*, 2013, **88**, 085318.
6 J. Kim, C. Jin, B. Chen, H. Cai, T. Zhao, P. Lee, S. Kahn, K. Watanabe, T. Taniguchi, S. Tongay, M. F. Crommie and F. Wang, Observation of ultralong valley lifetime in WSe_2/MoS_2 heterostructures, *Sci. Adv.*, 2017, **3**, e1700518.
7 C. Jin, J. Kim, M. Iqbal Bakti Utama, E. C. Regan, H. Kleemann, H. Cai, Y. Shen, M. J. Shinner, A. Sengupta, K. Watanabe, T. Taniguchi, S. Tongay, A. Zettl and F. Wang, Imaging of pure spin-valley diffusion current in WS_2-WSe_2 heterostructures, *Science*, 2018, **360**, 893–896.
8 P. Rivera, K. L. Seyler, H. Yu, J. R. Schaibley, J. Yan, D. G. Mandrus, W. Yao and X. Xu, Valley-polarized exciton dynamics in a 2D semiconductor heterostructure, *Science*, 2016, **351**, 688–691.
9 A. Ciarrocchi, D. Unuchek, A. Avsar, K. Watanabe, T. Taniguchi and A. Kis, Polarization switching and electrical control of interlayer excitons in two-dimensional van der Waals heterostructures, *Nat. Photonics*, 2019, **13**, 131–136.
10 W. T. Hsu, L. S. Lu, P. H. Wu, M. H. Lee, P. J. Chen, P. Y. Wu, Y. C. Chou, H. T. Jeng, L. J. Li, M. W. Chu and W. H. Chang, Negative circular polarization emissions from $WSe_2/MoSe_2$ commensurate heterobilayers, *Nat. Commun.*, 2018, **9**, 1356.
11 A. T. Hanbicki, H. J. Chuang, M. R. Rosenberger, C. S. Hellberg, S. V. Sivaram, K. M. McCreary, I. I. Mazin and B. T. Jonker, Double Indirect Interlayer Exciton in a $MoSe_2/WSe_2$ van der Waals Heterostructure, *ACS Nano*, 2018, **12**, 4719–4726.
12 M. Okada, A. Kutana, Y. Kureishi, Y. Kobayashi, Y. Saito, T. Saito, K. Watanabe, T. Taniguchi, S. Gupta, Y. Miyata, B. I. Yakobson, H. Shinohara and R. Kitaura, Direct and Indirect Interlayer Excitons in a van der Waals Heterostructure of hBN/WS_2/MoS_2/hBN, *ACS Nano*, 2018, **12**, 2498–2505.
13 J. Zhang, L. Du, S. Feng, R. W. Zhang, B. Cao, C. Zou, Y. Chen, M. Liao, B. Zhang, S. A. Yang, G. Zhang and T. Yu, Enhancing and controlling valley magnetic response in MoS_2/WS_2 heterostructures by all-optical route, *Nat. Commun.*, 2019, **10**, 4226.
14 K. F. Mak, K. He, J. Shan and T. F. Heinz, Control of valley polarization in monolayer MoS_2 by optical helicity, *Nat. Nanotechnol.*, 2012, **7**, 494–498.
15 H. Zeng, J. Dai, W. Yao, D. Xiao and X. Cui, Valley polarization in MoS_2 monolayers by optical pumping, *Nat. Nanotechnol.*, 2012, **7**, 490–493.
16 Y. Li, J. Ludwig, T. Low, A. Chernikov, X. Cui, G. Arefe, Y. D. Kim, A. M. Van Der Zande, A. Rigosi, H. M. Hill,

S. H. Kim, J. Hone, Z. Li, D. Smirnov and T. F. Heinz, Valley splitting and polarization by the Zeeman effect in monolayer $MoSe_2$, *Phys. Rev. Lett.*, 2014, **113**, 1–5.

17 A. Srivastava, M. Sidler, A. V. Allain, D. S. Lembke, A. Kis and A. Imamoğlu, Valley Zeeman effect in elementary optical excitations of monolayer WSe_2, *Nat. Phys.*, 2015, **11**, 141–147.

18 G. Aivazian, Z. Gong, A. M. Jones, R. L. Chu, J. Yan, D. G. Mandrus, C. Zhang, D. Cobden, W. Yao and X. Xu, Magnetic control of valley pseudospin in monolayer WSe_2, *Nat. Phys.*, 2015, **11**, 148–152.

19 D. Macneill, C. Heikes, K. F. Mak, Z. Anderson, A. Kormányos, V. Zólyomi, J. Park and D. C. Ralph, Breaking of valley degeneracy by magnetic field in monolayer $MoSe_2$, *Phys. Rev. Lett.*, 2015, **114**, 1–5.

20 L. Xu, M. Yang, L. Shen, J. Zhou, T. Zhu and Y. P. Feng, Large valley splitting in monolayer WS_2 by proximity coupling to an insulating antiferromagnetic substrate, *Phys. Rev. B*, 2018, **97**, 2–7.

21 H. Yu, G. B. Liu, P. Gong, X. Xu and W. Yao, Dirac cones and Dirac saddle points of bright excitons in monolayer transition metal dichalcogenides, *Nat. Commun.*, 2014, **5**, 1–7.

22 H. Yu, X. Cui, X. Xu and W. Yao, Valley excitons in two-dimensional semiconductors, *Natl. Sci. Rev.*, 2015, **2**, 57–70.

23 C. Robert, D. Lagarde, F. Cadiz, G. Wang, B. Lassagne, T. Amand, A. Balocchi, P. Renucci, S. Tongay, B. Urbaszek and X. Marie, Exciton radiative lifetime in transition metal dichalcogenide monolayers, *Phys. Rev. B*, 2016, **93**, 1–10.

24 G. Berghäuser, P. Steinleitner, P. Merkl, R. Huber, A. Knorr and E. Malic, Mapping of the dark exciton landscape in transition metal dichalcogenides, *Phys. Rev. B*, 2018, **98**, 1–6.

25 X. X. Zhang, Y. You, S. Y. F. Zhao and T. F. Heinz, Experimental Evidence for Dark Excitons in Monolayer WSe_2, *Phys. Rev. Lett.*, 2015, **115**, 1–6.

26 Z. Li, T. Wang, C. Jin, Z. Lu, Z. Lian, Y. Meng, M. Blei, S. Gao, T. Taniguchi, K. Watanabe, T. Ren, S. Tongay, L. Yang, D. Smirnov, T. Cao and S. F. Shi, Emerging photoluminescence from the dark-exciton phonon replica in monolayer WSe_2, *Nat. Commun.*, 2019, **10**, 1–7.

27 M. R. Molas, C. Faugeras, A. O. Slobodeniuk, K. Nogajewski, M. Bartos, D. M. Basko and M. Potemski, Brightening of dark excitons in monolayers of semiconducting transition metal dichalcogenides, *2D Mater.*, 2017, **4**, 021003.

28 X. X. Zhang, T. Cao, Z. Lu, Y. C. Lin, F. Zhang, Y. Wang, Z. Li, J. C. Hone, J. A. Robinson, D. Smirnov, S. G. Louie and T. F. Heinz, Magnetic brightening and control of dark excitons in monolayer WSe_2, *Nat. Nanotechnol.*, 2017, **12**, 883–888.

29 R. Vasconcelos, H. Bragança, F. Qu and J. Fu, Dark exciton brightening and its engaged valley dynamics in monolayer WSe_2, *Phys. Rev. B*, 2018, **98**, 195302.

30 M. Feierabend, S. Brem, A. Ekman and E. Malic, Brightening of spin- and momentum-dark excitons in transition metal dichalcogenides, *2D Mater.*, 2021, **8**, 015013.

31 A. Arora, T. Dixit, K. V. Anil Kumar, S. Krishnan, K. Lakshmi Ganapathi, A. Krishnan, P. K. Nayak and M. S. Ramachandra Rao, Plasmon induced brightening of dark exciton in monolayer WSe_2 for quantum optoelectronics, *Appl. Phys. Lett.*, 2019, **114**, 201101.

32 L. Du, J. Tang, J. Liang, M. Liao, Z. Jia, Q. Zhang, Y. Zhao, R. Yang, D. Shi, L. Gu, J. Xiang, K. Liu, Z. Sun and G. Zhang, Giant Valley Coherence at Room Temperature in 3R WS_2 with Broken Inversion Symmetry, *Research*, 2019, **2019**, 1–8.

33 P. K. Barman, P. V. Sarma, M. M. Shaijumon and R. N. Kini, High degree of circular polarization in WS_2 spiral nanostructures induced by broken symmetry, *Sci. Rep.*, 2019, **9**, 1–7.

34 S. Tongay, W. Fan, J. Kang, J. Park, U. Koldemir, J. Suh, D. S. Narang, K. Liu, J. Ji, J. Li, R. Sinclair and J. Wu, Tuning interlayer coupling in large-area heterostructures with CVD-grown MoS_2 and WS_2 monolayers, *Nano Lett.*, 2014, **14**, 3185–3190.

35 K. F. Mak, K. He, C. Lee, G. H. Lee, J. Hone, T. F. Heinz and J. Shan, Tightly bound trions in monolayer MoS_2, *Nat. Mater.*, 2013, **12**, 207–211.

36 H. Zeng, J. Dai, W. Yao, D. Xiao and X. Cui, Valley polarization in MoS_2 monolayers by optical pumping, *Nat. Nanotechnol.*, 2012, **7**, 490–493.

37 B. Zhu, H. Zeng, J. Dai, Z. Gong and X. Cui, Anomalously robust valley polarization and valley coherence in bilayer WS_2, *Proc. Natl. Acad. Sci. U. S. A.*, 2014, **111**, 11606–11611.

38 P. K. Nayak, F. C. Lin, C. H. Yeh, J. S. Huang and P. W. Chiu, Robust room temperature valley polarization in monolayer and bilayer WS_2, *Nanoscale*, 2016, **8**, 6035–6042.

39 Z. Li, G. Ezhilarasu, I. Chatzakis, R. Dhall, C. C. Chen and S. B. Cronin, Indirect Band Gap Emission by Hot Electron Injection in Metal/MoS_2 and Metal/WSe_2 Heterojunctions, *Nano Lett.*, 2015, **15**, 3977–3982.

40 G. Kioseoglou, A. T. Hanbicki, M. Currie, A. L. Friedman, D. Gunlycke and B. T. Jonker, Valley polarization and intervalley scattering in monolayer MoS_2, *Appl. Phys. Lett.*, 2012, **101**, 221907.

41 T. Korn, S. Heydrich, M. Hirmer, J. Schmutzler and C. Schller, Low-temperature photocarrier dynamics in monolayer MoS_2, *Appl. Phys. Lett.*, 2011, **99**, 2–5.

42 M. Amani, D. H. Lien, D. Kiriya, J. Xiao, A. Azcatl, J. Noh, S. R. Madhvapathy, R. Addou, K. C. Santosh, M. Dubey, K. Cho, R. M. Wallace, S. C. Lee, J. H. He, J. W. Ager, X. Zhang, E. Yablonovitch and A. Javey, Near-unity photoluminescence quantum yield in MoS_2, *Science*, 2015, **350**, 1065–1068.

43 K. Wang, B. Huang, M. Tian, F. Ceballos, M. W. Lin, M. Mahjouri-Samani, A. Boulesbaa, A. A. Puretzky, C. M. Rouleau, M. Yoon, H. Zhao, K. Xiao, G. Duscher and D. B. Geohegan, Interlayer Coupling in Twisted WSe_2/WS_2 Bilayer Heterostructures Revealed by Optical Spectroscopy, *ACS Nano*, 2016, **10**, 6612–6622.

44 F. Ceballos, M. Z. Bellus, H. Y. Chiu and H. Zhao, Ultrafast charge separation and indirect exciton formation in a MoS_2-$MoSe_2$ van der waals heterostructure, *ACS Nano*, 2014, **8**, 12717–12724.